Characterisation of a counting imaging detector for electron detection in the energy range 10-20 keV

Moldovan, G.; Sikharulidze, I.; Matheson, J.; Derbyshire, G.; Kirkland, A.I.; Abrahams, J.P.

Nuclear Instruments and Methods in Physics Research A 681 (2012) 21–24

Contents lists available at SciVerse ScienceDirect

Nuclear Instruments and Methods in Physics Research A

journal homepage: www.elsevier.com/locate/nima

Characterisation of a counting imaging detector for electron detection in the energy range 10–20 keV

G. Moldovan [a,*], I. Sikharulidze [b,1], J. Matheson [c], G. Derbyshire [c], A.I. Kirkland [a], J.P. Abrahams [b]

[a] University of Oxford, Department of Materials, Parks Road, Oxford OX1 3PH, UK
[b] Leiden University, Leiden Institute of Chemistry, P.O. Box 9502, 2300RA Leiden, The Netherlands
[c] Science and Technology Facilities Council, Rutherford Appleton Laboratory, Chilton, Didcot OX11 0QX, UK

ARTICLE INFO

Article history:
Received 9 March 2012
Accepted 20 March 2012
Available online 30 March 2012

Keywords:
Hybrid active pixel sensor
Electron detection
Imaging detectors

ABSTRACT

As part of a feasibility study into the use of novel electron detector for X-ray photoelectron emission microscopes (XPEEM) and related methods, we have characterised the imaging performance of a counting Medipix 2 readout chip bump bonded to a Silicon diode array sensor and directly exposed to electrons in the energy range 10–20 keV. Detective Quantum Efficiency (DQE), Modulation Transfer Function (MTF) and Noise Power Spectra (NPS) are presented, demonstrating very good performance for the case of electrons with an energy of 20 keV. Significant reductions in DQE are observed for electrons with energy of 15 keV and less, down to levels of 20% for electrons of 10 keV.

1. Introduction

With increased adoption of CMOS technologies in scientific instrumentation, a new degree of sophistication and speed is available to imaging detectors in conventional applications. One of the effects of this new technology is a change in the traditional barriers between flux integrating and particle counting imaging detectors. Whereas particle counting imaging detectors used to be too slow for high-flux operation, with in-pixel counters it is now possible to detect individual particles at high rates, and thus bring the benefits of single particle detection to many more imaging applications.

A family of applications that could benefit from this transition relates to surface imaging using low energy electrons, which include Low Energy Electron Microscopy (LEEM), Photo-Emission Electron Microscopy (PEEM) and X-Ray Photo-Emission Electron Microscopy (XPEEM) [1–3]. These require detection of electrons in the 10–20 keV energy range with high Detective Quantum Efficiency and high Modulation Transfer Function. Previous work on flux integrating detection has shown that an indirect system using Micro Channel Plates (MCP), scintillators with corresponding optics and Charge Coupled Device (CCD) detector suffer from very poor DQE and MTF. Significant improvements can be obtained using a direct detector system using a Monolithic Active Pixel Sensor (MAPS), but still the DQE was found to decrease with increasing spatial frequency above ~ 10 lp/mm [4,5].

The purpose of this work is to evaluate, in the same energy range, a counting hybrid active pixel sensor based on the Medipix chip [6,7]. This sensor has been evaluated qualitatively in previous work [8,9] and we have performed a quantitative evaluation in the present work. A Silicon diode array sensor coupled to a Medipix 2 device has been tested under direct exposure to electrons, and its performance has been fully characterised using the standard edge method [10].

2. Experimental

A dedicated vacuum system with a Kimball Physics EMG4212 monochromatic electron gun was used, the same as in previous work [4,5,11]. Uniform illumination on the imaging detector was obtained using a large spot size, and the beam current was controlled using the gun grid voltage and filament current. Electron flux at the detector input was measured using a calibrated AXUV-100 diode from International Radiation Detectors read with a Keithley 6517A electrometer [4,12].

The electron gun does also produce light that can complicate the analysis, and therefore most of this light was filtered away by mounting the detector off-axis and deflecting the electron beam onto it, using the built-in deflection electrodes in the gun. Detector parameters were set such that negligible counting was produced under dark conditions, i.e. with the gun on and the electrons deflected away from the imaging detector. The calibrated diode was of a type incorporating an Al coating, and was not, therefore, affected by the remnant light.

* Corresponding author. Tel.: +44 1865 273661; fax: +44 1865 273789.
E-mail address: grigore.moldovan@materials.ox.ac.uk (G. Moldovan).
[1] Current address: Diamond Light Source, Harwell Science and Innovation Campus, Didcot OX11 0DE, United Kingdom.

0168-9002/$ - see front matter Crown Copyright © 2012 Published by Elsevier B.V. All rights reserved.
http://dx.doi.org/10.1016/j.nima.2012.03.033

The Medipix 2 CMOS chip bump bonded to a 300 μm thick Si diode array sensor was used under direct illumination to electrons. The full pixel array contains 256×256 pixels, with a pixel size of $55\ \mu m \times 55\ \mu m$ each and a total sensitive area of $14\ mm \times 14\ mm$ [6,7]. The Medpix 2 chip was wire bonded to a CERN carrier board, which was connected to a computer with USB 1.1 board for readout and control [13]. The entire assembly was mounted on a CF100 flange and kept under vacuum. Pixelman software was used for data acquisition [14], and custom ImageJ plugins were developed for data analysis [15]. The sensor bias was set to a maximal level of 100 V provided by the USB readout board for highest sensitivity [8,9]. A single low threshold was employed to remove noise from the electron induced signal.

As required by the usual edge method, a straight opaque shadow mask was placed a few millimetres above the sensor, aligned at $\sim 3^\circ$ away from one axis of the pixel array. Aluminium was chosen as the mask material to minimise Bremsstrahlung emission, and a bevelled edge was used to avoid electron scatter. This edge mask was removed during acquisition of flat field, i.e. white noise, images. A standard Medipix 2 normalising procedure was employed to improve pixel response uniformity across the device, and electron hit rates were chosen such as to avoid pile-up for the Medipix 2 count rate. Full threshold sweeps were recorded for each electron energy under flat field illumination.

3. Results

Energy deposition spectra were obtained from threshold sweeps by differentiation. Given the monochromatic source of electrons used here, it is simple to identify the full energy deposition peak, and therefore calibrate threshold values in energy units, as presented in Fig. 1. The calibration for this detector was found to be

$$E = -0.163T + 73.98 \quad (1)$$

where E is electron energy in keV and T is threshold in digital DAC values.

A sequence of dark images, flat fields and edge images was recorded at each energy for 10 keV, 15 keV, and 20 keV electrons. A synthetic numerical test was run in parallel to generate input images for an ideal detector. Standard dark and bright corrections were used to remove any remnant non-uniformity in pixel response; a section of a typical edge image is shown magnified in Fig. 2. Exact positions and orientations of the edge were determined

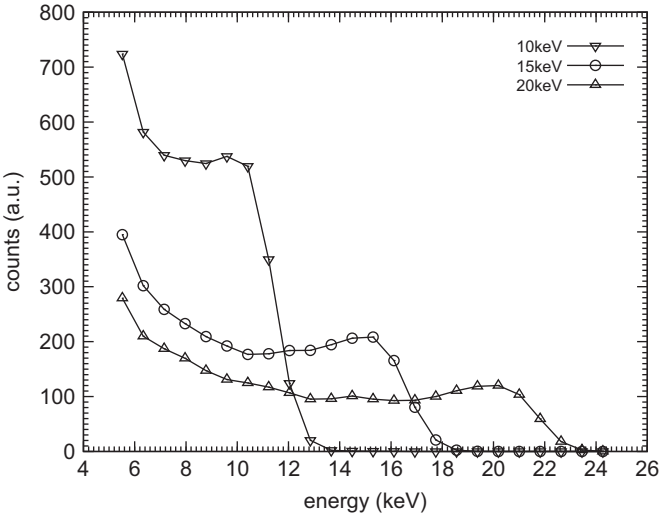

Fig. 1. Energy deposition spectra, as a function of electron energy.

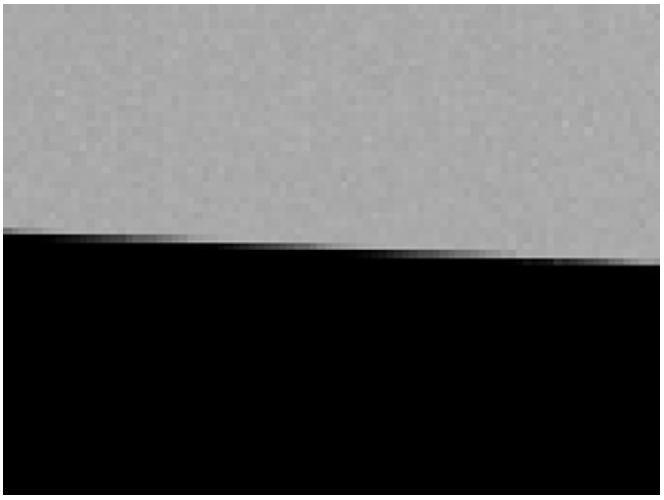

Fig. 2. Typical edge image of the shadow mask, recorded using electrons with an energy of 20 keV.

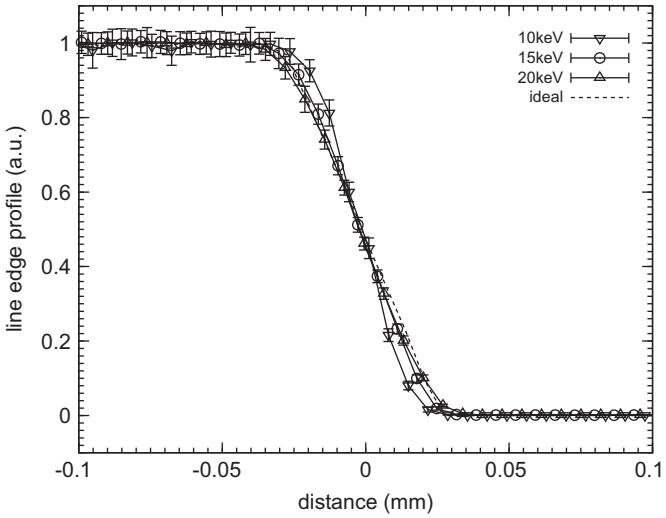

Fig. 3. Line Edge Profiles, as a function of electron energy. The ideal behaviour is included for reference only.

for each experimental condition, and oversampled line edge profiles were obtained by interpolation (Fig. 3). Care was taken that data was acquired away from the edge position until no further variations in intensity were observed, such that all low spatial frequencies were sampled.

An oversampled Line Spread Function (LSF) was obtained by differentiation, and resultant functions are displayed in Fig. 4 for each electron energy. Symmetry in the LSF provides assurance that electron scatter at the mask edge is minimal and therefore does not distort the edge profile. The modulation Transfer Function (MTF) was calculated from this, and is shown in Fig. 5 without any bandwidth corrections.

The Normalised Noise Power Spectrum (NNPS) was determined from flat field images using the standard frequency analysis and the gain values measured using the calibrated diodes (Fig. 6). MTF and NNPS were used to calculate Detective Quantum Efficiency (DQE) at each electron energy, as displayed in Fig. 7. Raw DQE is presented here, without a correction for pixel sampling, as the active area of these pixels is not known with sufficient precision.

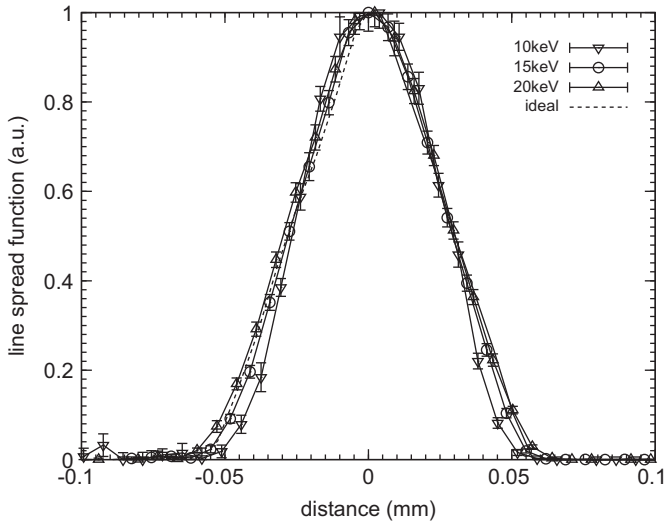

Fig. 4. Line Spread Functions, as a function of electron energy. The ideal behaviour is included for reference only.

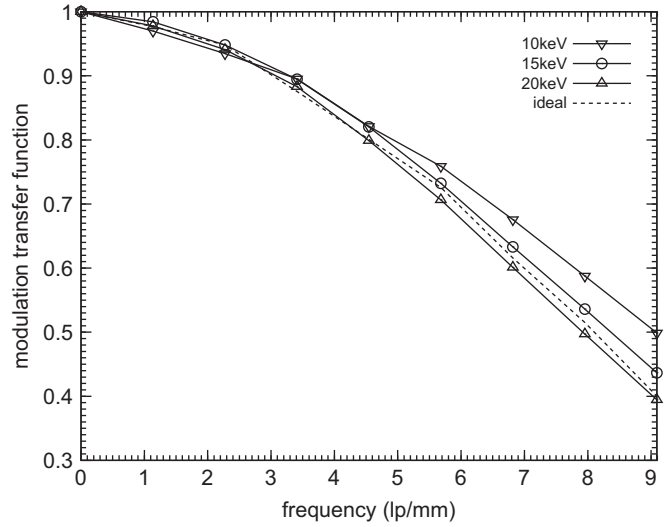

Fig. 5. Modulation Transfer Functions, as a function of electron energy. The ideal behaviour is included for reference only.

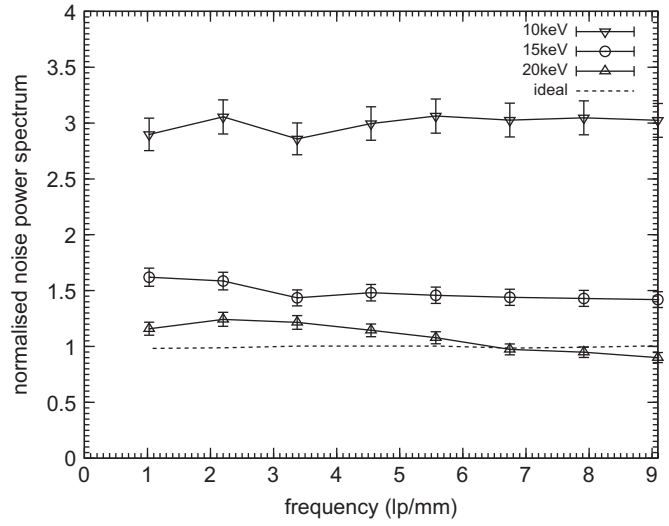

Fig. 6. Normalised Noise Power Spectra, as a function of electron energy. The ideal behaviour is included for reference only.

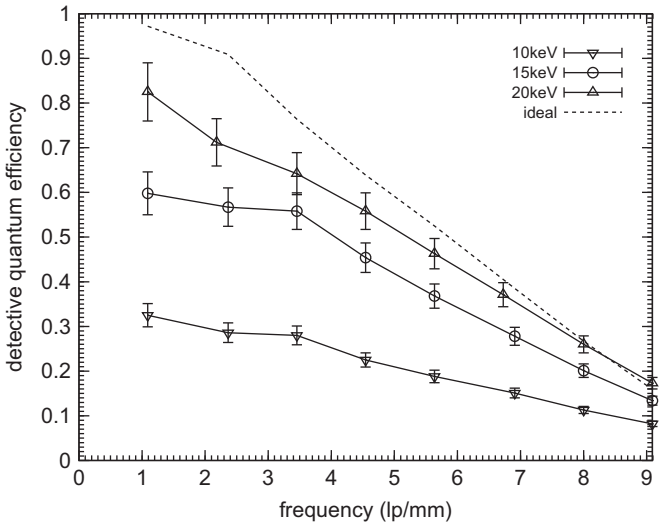

Fig. 7. Detective Quantum Efficiency, as a function of electron energy. The ideal behaviour is included for reference only.

4. Discussion

In agreement with previous work, the energy deposition spectra can be observed down to 5 keV [9]. Whilst this provides a statistical method to determine the energy of a beam of monochromatic electrons, energy determination for each electron is rather limited because of the wide and overlapping intrinsic distributions of the corresponding absorbed energies. This prevents the use of an energy window to filter away electrons of unwanted energy. It is possible nevertheless to define a threshold for suppression of electrons with lower energy, but only at the expense of efficiency, as spectra at higher energies are rather wide.

Very sharp edges are observed in the edge images, showing steps in line edge profiles close to one pixel. Only minor differences are observed between LSF and MTF at all electron energies used here, demonstrating very good resolution that does not vary significantly with electron energy. For the case of 10 keV electrons, MTF is slightly higher than that of an ideal imaging detector, indicating that the active area of these pixels is smaller than 100%. Whilst this may have a negative impact on the resultant DQE, it does show here as an improved MTF. MTF at high spatial frequencies for 20 keV is somewhat attenuated, indicating that the signal from single electrons is detected in several pixels.

NNPS shows somewhat noisy detection, with higher noise for the case of lower electron energies. This is associated with the expected signal/noise ratio for single electrons, indicating that for the case of 10 keV electrons, there is insufficient signal for adequate discrimination. High spatial frequency noise for the case of 20 keV electrons is attenuated, showing that at this energy signal from single electrons starts to trigger counting in more than one pixel.

The resultant DQE combines all these effects to show a very good performance for the case of 20 keV electrons, close to that of an ideal detector and probably limited only by the yield of backscattered electrons. DQE is much reduced at lower electron energies, associated with the increased noise displayed in NNPS. Overall, there is a strong correlation between DQE and electron energy, which would probably limit the application of this detector to electron energies higher than 10 keV.

5. Conclusion

Detailed quantification of low energy electron detection with a Medipix 2 counting imaging detector has been presented for electrons with energy in the 10–20 keV range. Very good Modulation Transfer Function was found at all electron energies investigated here, if somewhat limited by the 55 μm pixel pitch to 9.1 lpm. However, electrons with energy less than 15 keV do not provide sufficient signal for adequate signal/noise discrimination, as illustrated by Normalised Noise Power Spectra. The resultant Detective Quantum Efficiency depends very strongly on electron energy, with very good values for electrons of higher energy, but rather limited performance for the case of electrons of low energy.

Overall, very good detective performance was measured for the case of 20 keV electrons, but rather mixed performance was found for electrons of energy less than 15 keV.

Acknowledgments

This work was supported under Dutch Foundation for Technical Sciences STW grant LBB.7326, The Netherlands Organisation for Scientific Research NWO-Groot grant ESCHER, the Cyttron consortium, the CCLRC CfI programme, and EPSRC grants EP/C009509/1 and EP/H02834X/1. I.S. would like to thank Sense Jan van der Molen (Leiden University, The Netherlands), Raoul van Gastel (University of Twente, The Netherlands) and the Medipix Consortium for their support in experiment preparation.

References

[1] E. Bauer, Surface Science 299–300 (1994) 102, http://dx.doi.org/10.1016/0039-6028(94)90649-1.
[2] E. Bauer, Journal of Electron Spectroscopy 114–116 (2001) 975, http://dx.doi.org/10.1016/S0368-2048(00)00261-9.
[3] W. Swiech, G. Fecher, C. Ziethen, O. Schmidt, G. Schnhense, K. Grzelakowski, C.M. Schneider, R. Frmter, H. Oepen, J. Kirschner, Journal of Electron Spectroscopy 84 (1997) 171, http://dx.doi.org/10.1016/S0368-2048(97)00022-4.
[4] G. Moldovan, J. Matheson, G. Derbyshire, A. Kirkland, Nuclear Instruments and Methods in Physics Research, Section A 596 (2008) 402, http://dx.doi.org/10.1016/j.nima.2008.08.057.
[5] J. Matheson, G. Moldovan, A. Clark, M. Prydderch, R. Turchetta, G. Derbyshire, A. Kirkland, N. Allinson, Nuclear Instruments and Methods in Physics Research, Section A 608 (2009) 199, http://dx.doi.org/10.1016/j.nima.2009.06.065.
[6] X. Llopart, M. Campbell, Nuclear Instruments and Methods in Physics Research, Section A 509 (2003) 157, http://dx.doi.org/10.1016/S0168-9002(03)01565-1.
[7] 〈http://medipix.web.cern.ch〉.
[8] R. van Gastel, I. Sikharulidze, S. Schramm, J. Abrahams, B. Poelsema, R. Tromp, S. van der Molen, Ultramicroscopy 110 (2009) 33, http://dx.doi.org/10.1016/j.ultramic.2009.09.002.
[9] I. Sikharulidze, R. van Gastel, S. Schramm, J. Abrahams, B. Poelsema, R. Tromp, S. van der Molen, Nuclear Instruments and Methods in Physics Research, Section A 633 (Supplement 1) (2011) S239, http://dx.doi.org/10.1016/j.nima.2010.06.177.
[10] R.R. Meyer, A.I. Kirkland, Microscopy Research and Technique 49 (2000) 269.
[11] 〈http://www.kimballphysics.com〉.
[12] 〈http://www.ird-inc.com〉.
[13] Z. Vykydal, J. Jakubek, S. Pospisil, Nuclear Instruments and Methods in Physics Research, Section A 563 (2006) 112, http://dx.doi.org/10.1016/j.nima.2006.01.114.
[14] T. Holy, J. Jakubek, S. Pospisil, J. Uher, D. Vavrik, Z. Vykydal, Nuclear Instruments and Methods in Physics Research, Section A 563 (2006) 254 http://dx.doi.org/10.1016/j.nima.2006.01.122.
[15] M.D. Abramoff, P.J. Magelhaes, S.J. Ram, Biophoton International 11 (2004) 36.